EUROPHYSICS LETTERS 15 January 2006

Europhys. Lett., **73** (2), pp. 211–217 (2006)
DOI: 10.1209/epl/i2005-10387-4

Field description and electron acceleration of focused flattened Gaussian laser beams

W. WANG[1,2], P. X. WANG[1](*), Y. K. HO[1], Q. KONG[1], Z. CHEN[1], Y. GU[2] and S. J. WANG[2]

[1] *Institute of Modern Physics, Fudan University - Shanghai, 200433, PRC*
[2] *Shanghai Institute of Laser Plasma - Shanghai, 201800, PRC*

received 7 August 2005; accepted in final form 23 November 2005
published online 16 December 2005

PACS. 42.60.Jf – Beam characteristics: profile, intensity, and power; spatial pattern formation.
PACS. 41.85.Ja – Beam transport.
PACS. 41.75.Jv – Laser-driven acceleration.

Abstract. – By using the superposition of N suitably weighted Laguerre-Gaussian beams, the analytical expressions of all six electromagnetic field components of focused Flattened Gaussian Beams (FGBs) are obtained in the Lorentz gauge. The phase velocity distributions of the field near the focus of FGBs propagating in vacuum are investigated. There exists a subluminous wave phase velocity region surrounding the laser beam axis. We further apply this focused FGB to vacuum laser acceleration. As with the focused Standard Gaussian Beam (SGB), electrons injected into the focused FGB can be captured in the acceleration phase and then violently accelerated.

In recent years, the rapid development of intense laser technology [1] has stimulated the creation of many frontier research areas [2]. Among them, the laser acceleration of electrons has received wide attention [3–6]. In our previous works, a unique vacuum laser acceleration scheme, the Capture and Acceleration Scenario (CAS) [7] has been proposed. Results were obtained in a Standard Gaussian Beam (SGB), *i.e.*, a TEM_{00} mode Gaussian beam and the CAS can work only when the laser field is strong enough [8]. We notice that, in order to extract as much energy as possible while minimizing the undesirable effects often associated with high peak power (*e.g.*, self-focusing and optical damage), the radial intensity distribution of real ultra-high intensity laser beam is always of a flat-topped profile, *i.e.*, a distribution which is nearly uniform over the central region and reducing smoothly to zero [9]. How to describe this type of laser beam is an important question. During the past two decades, much effort has been made in this direction, but difficulties still exist. Gori proposed a novel approach to the description of one electromagnetic field component for Flattened Gaussian Beams (FGBs) [10]. Its attractive advantage is that it can be expressed as a finite superposition of suitably weighted Laguerre-Gaussian (LG) beams. Because LG beams are eigen solutions of the paraxial wave equation, thus, the evaluation of the field across any plane z can be

(*) E-mail: wpx@fudan.edu.cn

done in an exact and simple way by using the propagation law for LG beams [11–13]. What Gori concerned about in his paper is the distribution of light intensity and obtaining one main transverse component, *i.e.* the electric field component is enough. We know that, simply from one electric field component, it is hard to obtain all other five electromagnetic field components which satisfy *Maxwell* equations. Normally, $\nabla \cdot \boldsymbol{E} = 0$ and $\partial \boldsymbol{B}/\partial t = -\nabla \times \boldsymbol{E}$ are adopted to obtain the analytical expressions of other five components, but solving them beyond a plane wave is almost impossible even if under paraxial approximation, especially for a pulsed laser beam. However, the exact expressions of all six electromagnetic field components of the field are needed for theoretical applications such as using 3D simulation to study the interaction between laser field and charged particles. Following the method introduced by Gori due to the same form of the wave equations in vacuum, we obtain a similar expression of the vector potential and derive all six electromagnetic field components of FGB in the Lorentz gauge. In acceleration experiments, FGB are commonly focused by an off-axial parabolic mirror, thus we derive all six electromagnetic field components of the focused FGB. They are analytically expressed and are therefore practical for many applications. And, we investigate the phase velocity distributions of the field near the focus of the focused FGBs propagating in vacuum. Using 3D test particle simulations, we further confirm that the CAS is still valid in this flat-topped laser beam.

Here we enact the vector potential $\boldsymbol{A}$ (A_x, $A_y = 0$, $A_z = 0$) of a FGB but not the electric field as ref. [10]. Due to the same form of the wave equations in vacuum, following the method introduced in ref. [10], the expression of the vector potential component A_x can also be expressed as the same form

$$\begin{aligned} A_x \;=\; & A_0 \frac{w_N(0)}{w_N(z)} \exp\left[-\frac{r^2}{w_N^2(z)}\right] \exp\left[i\left[-\varphi_N(z) - \varphi_0 + \frac{kr^2}{2R_N(z)}\right]\right] \times \\ & \times \sum_{n=0}^{N} c_n^{(N)} L_n\left(\frac{2r^2}{w_N^2(z)}\right) \exp[-2in\varphi_N(z)] f(\eta) \exp[ik\eta], \end{aligned} \tag{1}$$

in which $f(\eta) = \exp[-(\eta/c\tau)^2]$ is the form factor of the laser pulse with τ being the pulse duration, $\eta = z - ct$, $k = 2\pi/\lambda$ the laser wave number. L_n is the n-th Laguerre polynomial, and the $c_n^{(N)}$ coefficient is defined as $c_n^{(N)} = (-1)^n \sum_{m=n}^{N} \binom{m}{n} \frac{1}{2^m}$, where $\binom{m}{n}$ denotes a binomial coefficient. The parameters $w_N(z)$, $R_N(z)$ and $\varphi_N(z)$ are given by $w_N(z) = w_N(0)[1 + (z/Z_R)^2]^{1/2}$, $R_N(z) = z[1 + (Z_R/z)^2]$ and $\varphi_N(z) = \tan^{-1}(z/Z_R)$, where $Z_R = kw_N^2(0)/2$ is the Rayleigh length, $w_N(0) = w_0/\sqrt{N+1}$ is the waist size of all LG beams and w_0 is the waist size of the FGB.

For an optical system consisting of one thin converging lens with focal length f placed in the input plane and the output plane at a distance z beyond the lens, the $ABCD$ matrix [13] will be given by the product of the matrices corresponding to the thin lens and free propagation; it is

$$\begin{bmatrix} A & B \\ C & D \end{bmatrix} = \begin{bmatrix} 1 & z \\ 0 & 1 \end{bmatrix} \begin{bmatrix} 1 & 0 \\ -\dfrac{1}{f} & 1 \end{bmatrix} = \begin{bmatrix} 1 - \dfrac{z}{f} & z \\ -\dfrac{1}{f} & 1 \end{bmatrix}. \tag{2}$$

Then we can get that the focused FGBs have the same form as eq. (1), but the parameters $w_N(z)$, $R_N(z)$ and $\varphi_N(z)$ are replaced by $w_N(z) = |A| w_N(0)(1 + G^2)^{1/2}$, $R_N(z) = AB\frac{1+G^{-2}}{1+BC(1+G^{-2})}$ and $\varphi_N(z) = \tan^{-1} G$, where $G = \frac{B}{A}\frac{2}{kw_N^2(0)}$, A, B and C are the elements of the pertaining $ABCD$ matrix. For convenience, eq. (1) can be rewritten as

$$A_x = \mathcal{A}_N(r, z, t) \mathcal{L}_N(r, z) f(\eta), \tag{3}$$

where

$$\mathcal{A}_N(r,z,t) \equiv A_0 \frac{w_N(0)}{w_N(z)} \exp\left(-\frac{r^2}{w_N^2(z)}\right) \exp\left(i\varphi^{(p)}(r,z,t)\right), \tag{4}$$

$$\varphi^{(p)}(r,z,t) \equiv k\eta - \varphi_N(z) - \varphi_0 + \frac{kr^2}{2R_N(z)}, \tag{5}$$

$$\mathcal{L}_N(r,z) \equiv \sum_{n=0}^{N} c_n^{(N)} L_n\left(\frac{2r^2}{w_N^2(z)}\right) \exp[-2in\varphi_N(z)], \tag{6}$$

and define

$$\mathcal{L}_N^{(1)}(r,z) \equiv \sum_{n=0}^{N} c_n^{(N)} L_n^{(1)}\left(\frac{2r^2}{w_N^2(z)}\right) \exp[-2in\varphi_N(z)], \tag{7}$$

$$\mathcal{L}_N^{(2)}(r,z) \equiv \sum_{n=0}^{N} c_n^{(N)} L_{n-1}^{(2)}\left(\frac{2r^2}{w_N^2(z)}\right) \exp[-2in\varphi_N(z)], \tag{8}$$

$$\mathcal{L}n_N(r,z) \equiv \sum_{n=0}^{N} nc_n^{(N)} L_n\left(\frac{2r^2}{w_N^2(z)}\right) \exp[-2in\varphi_N(z)], \tag{9}$$

$$\mathcal{L}n_N^{(1)}(r,z) \equiv \sum_{n=0}^{N} nc_n^{(N)} L_n^{(1)}\left(\frac{2r^2}{w_N^2(z)}\right) \exp[-2in\varphi_N(z)]. \tag{10}$$

For a pulsed laser beam polarized along the x-direction and propagating along the z-axis, the vector potential $\boldsymbol{A}$ and the scalar potential Φ can be assumed of the form [14]

$$\boldsymbol{A} = f(\eta)\Lambda_x(x,y,z)\exp[ik\eta]\hat{e}_x, \qquad \Phi = f(\eta)\Gamma(x,y,z)\exp[ik\eta], \tag{11}$$

where $\hat{e}_x$ is the unit vector representing the laser polarization direction. If the Lorentz gauge is used, we can get $\Phi = (c\partial A_x/\partial x)/[ik - 2\eta/(c\tau)^2]$. Once $\boldsymbol{A}$ is obtained, $\boldsymbol{E}$ and $\boldsymbol{B}$ can be derived by $\boldsymbol{E} = -\partial\boldsymbol{A}/\partial t - \nabla\Phi$ and $\boldsymbol{B} = \nabla \times \boldsymbol{A}$. Then, the electromagnetic components of the focused FGBs can be expressed as

$$\begin{aligned} E_x = &-\left(\frac{2\eta}{c\tau^2} - i\omega\right) f(\eta)\cdot\mathcal{A}_N(r,z,t)\cdot\mathcal{L}_N(r,z) - \\ &-\left\{\frac{2}{w_N^2(z)}\left[\mathcal{L}_N(r,z) - 2\mathcal{L}_N^{(1)}(r,z) + \frac{2x^2}{w_N^2(z)}\left(\mathcal{L}_N(r,z) + 4\mathcal{L}_N^{(2)}(r,z)\right)\right] - \frac{k^2x^2}{R_N^2(z)}\mathcal{L}_N(r,z) + \right. \\ &\left. + \frac{ik}{R_N(z)}\left[\mathcal{L}_N(r,z) + \frac{4x^2}{w_N^2(z)}\left(\mathcal{L}_N(r,z) - 2\mathcal{L}_N^{(1)}(r,z)\right)\right]\right\}\frac{cf(\eta)\mathcal{A}_N(r,z,t)}{ik - 2\eta/(c\tau)^2}, \end{aligned} \tag{12}$$

$$\begin{aligned} E_y = &-\left\{\frac{4}{w_N^4(z)}\left(\mathcal{L}_N(r,z) + 4\mathcal{L}_N^{(2)}(r,z)\right) - \frac{k^2}{R_N^2(z)}\mathcal{L}_N(r,z) + \right. \\ &\left. + \frac{4ik}{w_N^2(z)R_N(z)}\left(\mathcal{L}_N(r,z) - 2\mathcal{L}_N^{(1)}(r,z)\right)\right\}\frac{cxyf(\eta)\cdot\mathcal{A}_N(r,z,t)}{ik - 2\eta/(c\tau)^2}, \end{aligned} \tag{13}$$

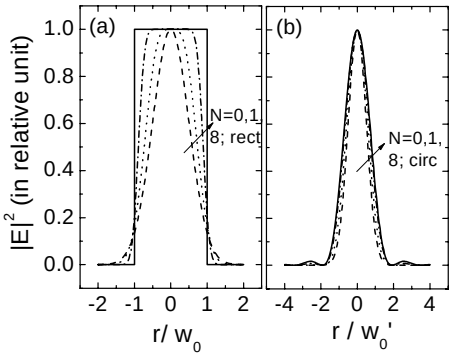

Fig. 1 – Intensity profiles of FGBs as a function of x for different values of N in the waist plane (a) and focal plane (b). (a) The solid line represents the rect function; (b) the solid line represents the circ function.

$$
\begin{aligned}
E_z \;=\; & -\Bigg\{\frac{1}{w_N^3(z)}\frac{\partial w_N(z)}{\partial z}\left[-6\left(\mathcal{L}_N(r,z)-2\mathcal{L}_N^{(1)}(r,z)\right)-\frac{4r^2}{w_N^2(z)}\left(\mathcal{L}_N(r,z)+4\mathcal{L}_N^{(2)}(r,z)\right)\right]+\\
& +\frac{2}{w_N^2(z)}\left[i\frac{\partial\varphi_N^{(p)}(r,z,t)}{\partial z}\left(\mathcal{L}_N(r,z)-2\mathcal{L}_N^{(1)}(r,z)\right)-\right.\\
& \left.-i2\frac{\partial\varphi_N(z)}{\partial z}\left[\mathcal{L}n_N(r,z)-2\mathcal{L}n_N^{(1)}(r,z)\right]-\frac{2\eta}{(c\tau)^2}\left[\mathcal{L}_N(r,z)-2\mathcal{L}_N^{(1)}(r,z)\right]\right]+\\
& +\frac{1}{w_N(z)}\frac{ik}{R_N(z)}\frac{\partial w_N(z)}{\partial z}\left[-\mathcal{L}_N(r,z)-\frac{2r^2}{w_N^2(z)}\left(\mathcal{L}_N(r,z)-2\mathcal{L}_N^{(1)}(r,z)\right)\right]+\\
& +\frac{2}{c(c\tau)^2}\frac{c}{ik-2\eta/(c\tau)^2}\left[\frac{2}{w_N^2(z)}\left(\mathcal{L}_N(r,z)-2\mathcal{L}_N^{(1)}(r,z)\right)+\frac{ik}{R_N(z)}\mathcal{L}_N(r,z)\right]+\\
& +\frac{k}{R_N(z)}\left[\frac{-i}{R_N(z)}\frac{\partial R_N(z)}{\partial z}\mathcal{L}_N(r,z)-\frac{\partial\varphi_N^{(p)}(r,z,t)}{\partial z}\mathcal{L}_N(r,z)+\right.\\
& \left.+2\frac{\partial\varphi_N(z)}{\partial z}\mathcal{L}n_N(r,z)-i\frac{2\eta}{(c\tau)^2}\mathcal{L}_N(r,z)\right]\Bigg\}\frac{cxf(\eta)\mathcal{A}_N(r,z,t)}{ik-2\eta/(c\tau)^2},
\end{aligned}
\tag{14}
$$

$$
B_x = 0, \tag{15}
$$

$$
\begin{aligned}
B_y \;=\; & \left\{\frac{1}{w_N(z)}\frac{\partial w_N(z)}{\partial z}\left[-\left(1+\frac{2r^2}{w_N^2(z)}\right)\mathcal{L}_N(r,z)+\frac{4r^2}{w_N^2(z)}\mathcal{L}_N^{(1)}(r,z)\right]+\right.\\
& \left.+i\frac{\partial\varphi_N^{(p)}(r,z,t)}{\partial z}\mathcal{L}_N(r,z)-i2\frac{\partial\varphi_N(z)}{\partial z}\mathcal{L}n_N(r,z)-\frac{2\eta}{(c\tau)^2}\mathcal{L}_N(r,z)\right\}f(\eta)\mathcal{A}_N(r,z,t),
\end{aligned}
\tag{16}
$$

$$
B_z = -\left[\frac{2}{w_N^2(z)}\left(\mathcal{L}_N(r,z)-2\mathcal{L}_N^{(1)}(r,z)\right)+\frac{ik}{R_N(z)}\mathcal{L}_N(r,z)\right]yf(\eta)\mathcal{A}_N(r,z,t). \tag{17}
$$

Figure 1 shows the intensity profiles of FGBs for several values of N in the waist plane (a) and focal plane (b). It can be seen that the curve is Gaussian for $N = 0$, the top of the curve becomes more and more flattened in the waist plane as N increases. When $N \to \infty$, the curve will tend to be a rect function (solid line; as usual, rect(r) is defined as 1 if $|r| \leq 1$ and 0

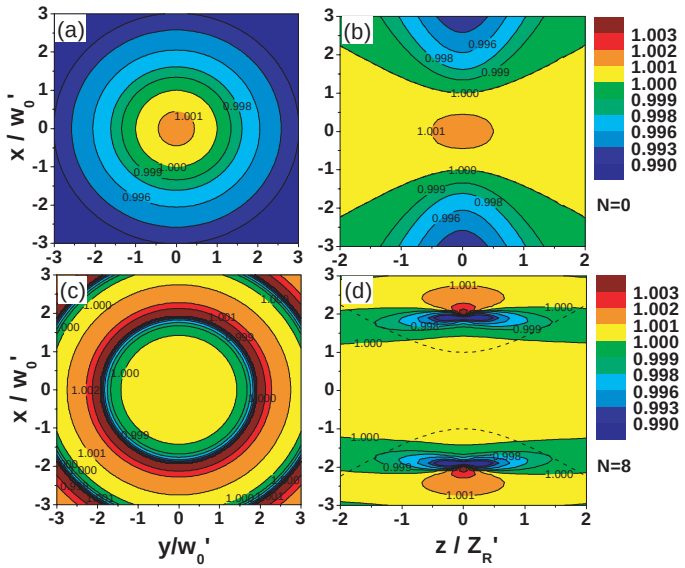

Fig. 2 – Distributions of the minimum phase velocity (in units of c) near the focus of FGBs. (a) $z = 0$ plane with $N = 0$, (b) $y = 0$ plane with $N = 0$, (c) $z = 0$ plane with $N = 8$, (d) $y = 0$ plane with $N = 8$. The dashed lines in (b) and (d) show the beam profiles.

elsewhere) in the waist plane or a circ function (solid line; defined as the Fourier transform of rect function) in the focal plane. From fig. 1(b) it can be noticed that, when $N > 0$, the intensity pattern in the focal plane has dark rings because of diffraction. In the following, we select a representative FGB with $N = 8$ to study the characteristics of the flat-topped laser beams. If the output beam of a given laser facility deviates from the 8th-order FGB, one can easily change N accordingly to make a more specific study.

The effective phase velocity of the wave along a particle trajectory $(V_\varphi)_l$ can be calculated using $\partial\varphi/\partial t + (V_\varphi)_l \cdot (\nabla\varphi)_l = 0$ [7], where φ is the phase of the wave, $(\nabla\varphi)_l$ is the phase gradient along the particle trajectory. The minimum phase velocity, normally called the phase velocity of the wave is $V_p = -(\partial\varphi/\partial t)|\nabla\varphi|$. Figure 2 shows the minimum phase velocity (in units of c) distributions of the focused FGBs near the focus for $N = 0$ ((a) and (b)) and $N = 8$ ((c) and (d)). The subluminous phase velocity region, namely, the phase velocity of the wave is less than c, can be found in the focused FGB ($N = 8$), but it is markedly different with that of SGB ($N = 0$). For $N = 0$, the subluminous phase velocity region emerges just beyond the beam width $w(z)$ (dashed line), and extends along the diffraction angle. While for $N = 8$, the subluminous phase velocity region exists between $r = w_0'$ and $2w_0'$, forming a hollow column (there are other subluminous phase velocity regions outside $2w_0'$, where the field intensity is very small).

The physical mechanism underlying the CAS is that when an electron is captured, the effective wave phase velocity along the dynamic trajectory of the captured particle can approach the light speed c, or even approach the speed of the particle [7]. Thus, the captured electron can be kept in the acceleration phase of the wave for a long time, and gain considerable energy from the laser field. In which, the longitudinal electric field of the laser beam is responsible for the energy gain in CAS. The subluminous phase velocity region associated with the longitudinal electric field may form a natural acceleration channel [7, 8]. Our calculation shows

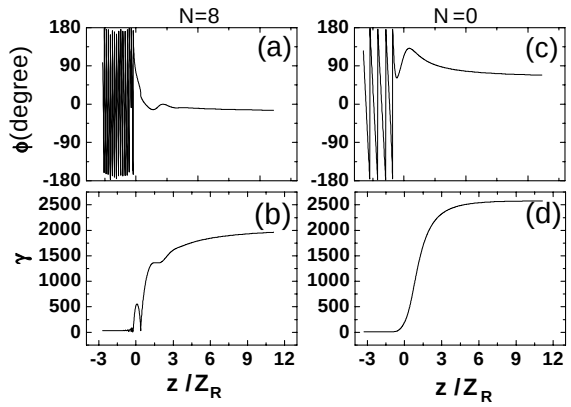

Fig. 3 – Typical electron dynamics in (a)-(b) focused FGB and in (c)-(d) focused SGB. Laser field intensity $a_0 = 80$, beam width at the focus $kw_0' = 60$, and pulse width $\omega\tau = 500$ are used for both cases. Electron initial momentum $P_0 = 9$ and 35, electron incident angle $\tan\theta = 0.12$ and 0.23 for $N = 0$ and 8, respectively. (a) and (c), laser wave phase experienced by the electron; (b) and (d), electron energy.

that the longitudinal electric field component (E_z) of focused FGBs with $N = 8$ is similar to that of SGB ($N = 0$). "Does the CAS scheme still hold in a focused FGB?" is also what we are concerned with in this letter. To answer this question we study the electron dynamics in the focused FGB propagating in vacuum using 3D test particle simulation to solve the relativistic Newton-Lorentz equation [7,8], $\mathrm{d}\boldsymbol{P}/\mathrm{d}t = -e(\boldsymbol{E} + \boldsymbol{v} \times \boldsymbol{B})$, where $\boldsymbol{v}$ is the electron velocity in units of c, $\boldsymbol{P} = \gamma\boldsymbol{v}$ is the electron momentum in units of $m_e c$, and $\gamma = (1 - v^2)^{-1/2}$ is the Lorentz factor. Simulations of electron dynamics in the focused FGB ($N = 8$) are performed at laser intensity $a_0 = 80$, where $a_0 \equiv eE_0/m_e\omega c$ is a dimensionless parameter measuring laser intensity, E_0 denotes the electric field amplitude of the laser beam at focus, ω the laser circular frequency, e and m_e the electron charge and rest mass, respectively. Other parameters are beam width at the focus $kw_0' = 60$, laser pulse width $\omega\tau = 500$, electron initial momentum $P_0 = 35$, electron incident crossing angle (relative to the laser beam direction) $\tan\theta = 0.23$. Results are shown in figs. 3(a) and (b). For comparison, the electron dynamics in SGB ($N = 0$) are also shown (figs. 3(c)-(d)). The SGB has the same a_0, w_0', and τ like the FGB ($N = 8$). However, P_0 and $\tan\theta$ are optimized to be 9 and 0.12, respectively. Results of these simulations indicate that CAS scheme still hold in a focused FGB.

In this letter, the characteristics of the focused FGB and electron dynamics in such a field are studied. The analytical expressions of all six electromagnetic field components of the focused FGBs are obtained. We found that for a focused FGB propagating in vacuum, there exists a subluminous wave phase velocity region surrounding the laser beam axis. Although there are marked differences between FGB and SGB, the vacuum electron acceleration scheme CAS found in SGB, is also valid in the focused FGBs.

* * *

The authors would like to thank L. J. Qian, X. L. Xie, and L. Xia for helpful discussions. This work is supported partly by the National Natural Science Foundation of China under Contracts No. 10475018 and No. 10335030, and by the National Key Basic Research Special Foundation (NKBRF) under Grant No. G1999075200.

REFERENCES

[1] Aoyama M., Yamakawa K., Akahane Y., Ma J., Inoue N., Ueda H. and Kiriyama H., *Opt. Lett.*, **28** (2003) 1594; Bahk S.-W., Rousseau P., Planchon T. A., Chvykov V., Kalintchenko G., Maksimchuk A., Mourou G. A. and Yanovsky V., *Opt. Lett.*, **29** (2004) 2837.

[2] Pukhov A., *Rep. Prog. Phys.*, **66** (2003) 47; Umstadter D., *J. Phys. D*, **36** (2003) R151.

[3] Tajima T. and Mourou G., *Phys. Rev. ST Accel. Beams*, **5** (2002) 031301.

[4] Mangles S. P. D., Murphy C. D., Najmudin Z., Thomas A. G. R., Collier J. L., Dangor A. E., Divall E. J., Foster P. S., Gallacher J. G., Hooker C. J., Jaroszynski D. A., Langley A. J., Mori W. B., Norreys P. A., Tsung F. S., Viskup R., Walton B. R. and Krushelnick K., *Nature*, **431** (2004) 535; Geddes C. G. R., Toth Cs., Tilborg J. van, Esarey E., Schroeder C. B., Bruhwiler D., Nieter C., Cary J. and Leemans W. P., *Nature*, **431** (2004) 538; Faure J., Glinec Y., Pukhov A., Kiselev S., Gordienko S., Lefebvre E., Rousseau J.-P., Burgy F. and Malka V., *Nature*, **431** (2004) 541.

[5] Salamin Y. I. and Keitel C. H., *Phys. Rev. Lett.*, **88** (2002) 095005; Salamin Y. I. and Keitel C. H., *Appl. Phys. Lett.*, **77** (2000) 1082; Salamin Y. I., *Phys. Lett. A*, **335** (2005) 289.

[6] Yu W., Bychenkov V., Sentoku Y., Yu M. Y., Sheng Z. M. and Mima K., *Phys. Rev. Lett.*, **85** (2000) 570.

[7] Wang P. X., Ho Y. K., Yuan X. Q., Kong Q., Cao N., Sessler A. M., Esarey E. and Nishida Y., *Appl. Phys. Lett.*, **78** (2001) 2253.

[8] Pang J., Ho Y. K., Yuan X. Q., Cao N., Kong Q., Wang P. X., Shao L., Esarey E. H. and Sessler A. M., *Phys. Rev. E*, **66** (2002) 066501.

[9] Silvestri S. De, Laporta P., Magni V., Svelto O. and Majocchi B., *Opt. Lett.*, **13** (1988) 201; Patterson F. G., Gonzales R. and Perry M. D., *Opt. Lett.*, **16** (1991) 1107.

[10] Gori F., *Opt. Commun.*, **107** (1994) 335.

[11] Bagini V., Borghi R., Gori F., Pacileo A. M., Santarsiero M., Ambrosini D. and Schirripa G., *J. Opt. Soc. Am. A*, **13** (1996) 1385.

[12] Santarsiero M., Aiello D., Borghi R. and Vicalvi S., *J. Mod. Opt.*, **44** (1997) 633.

[13] Siegman A. E., *Lasers* (University Science, Mill Valley) 1986, pp. 581-697.

[14] Wang P. X. and Wang J. X., *Appl. Phys. Lett.*, **81** (2002) 4473.